Available online at www.sciencedirect.com
SCIENCE DIRECT
Journal of African Earth Sciences 45 (2006) 333–346
Journal of African Earth Sciences
www.elsevier.com/locate/jafrearsci

# Geochemistry of an ultramafic-rodingite rock association in the Paleoproterozoic Dixcove greenstone belt, southwestern Ghana

Kodjopa Attoh [a,*], Matthew J. Evans [a,1], M.E. Bickford [b]

[a] Department of Earth and Atmospheric Sciences, Cornell University, Snee Hall, Ithaca, NY 14853, USA
[b] Department of Earth Sciences, Syracuse University, Syracuse, NY 13244, USA

Received 11 January 2005; received in revised form 20 February 2006; accepted 2 March 2006
Available online 18 May 2006

**Abstract**

Rodingite occurs in ultramafic rocks within the Paleoproterozoic (Birimian) Dixcove greenstone belt in southwestern Ghana. U–Pb analyses of zircons from granitoids intrusive into the greenstone belt constrain the age of the rodingite-ultramafic association to be older than 2159 Ma. The ultramafic complex consists of variably serpentinized dunite and harzburgite overlain by gabbroic rocks, which together show petrographic and geochemical characteristics consistent with their formation by fractional crystallization involving olivine and plagioclase cumulates. Major and trace element concentrations and patterns in the ultramafic–mafic cumulate rocks and associated plagiogranite are similar to rocks in ophiolitic suites. The rodingites, which occur as irregular pods and lenses, and as veins and blocks in the serpentinized zones, are characterized by high $Al_2O_3$ and CaO contents, which together with petrographic evidence indicate their formation from plagioclase-rich protoliths. The peridotites are highly depleted in REE and display flat, chondrite-normalized REE patterns with variable, but mostly small, positive Eu anomalies whereas the rodingites, which are also highly depleted, with overall REE contents from 0.04 to 1.2 times chondrite values, display distinct large positive Eu anomalies. It is proposed that the rodingite-bearing Birimian ultramafic complex and associated pillowed greenstone belt basalts may represent fragments of a Paleoproterozoic oceanic lithosphere.


*Keywords:* Paleoproterozoic; Ultramafic rocks; Rodingite; Birimian; West Africa

## 1. Introduction

Archean and Paleoproterozoic greenstone belt basalts appear to be products of subduction-related magmatism and have provided important information about crustal growth during early earth history (Condie, 1997). Ultramafic rocks, on the other hand, typically constitute only a minor component of such greenstone belts, but may also contain useful information on the tectonic regimes in which the early continental crust was assembled. This is because ultramafic rocks comprise essential lithologies of the ophiolitic suite which are considered diagnostic of subduction tectonic settings in Phanerozoic orogens (Pearce, 2003; Peters et al., 1991). In such settings ultramafic rocks with rodingites have proved diagnostic of obducted oceanic crust (Coleman, 1977). There is a special interest in ultramafic rocks associated with the Paleoproterozoic (Birimian) greenstone belts of the West African craton (WAC) because, together with the 2.0–2.2 Ga granitoids, they record one of the most extensive juvenile crust-forming events near the Archean–Proterozoic boundary (Hirdes and Davis, 2002; Attoh and Ekwueme, 1997; Taylor et al., 1992). However, there is disagreement about the tectonic setting where they formed, with some workers suggesting that Birimian juvenile crust production occurred largely in arc environments (e.g., Sylvester and Attoh, 1992; Ama Salah et al., 1996), while others have proposed that

* Corresponding author. Tel.: +1 607 255 1039; fax: +1 607 254 4780.
*E-mail address:* ka17@cornell.edu (K. Attoh).
[1] Present address: Department of Geology, College of William and Mary, P.O. Box 8795, Williamsburg, VA 23187 8795, USA.

1464-343X/$ - see front matter © 2006 Elsevier Ltd. All rights reserved.
doi:10.1016/j.jafrearsci.2006.03.010

it was plume generated (Abouchami et al., 1990). In this paper, we report the first field description, and present petrographic and geochemical data on ultramafic rocks and associated rodingites in a Birimian greenstone belt, and suggest that the ultramafic rocks together with related pillow basalts may represent fragments of a Paleoproterozoic oceanic crust.

## 2. Geological setting

Paleoproterozoic volcanic and sedimentary rocks comprise the extensive Birimian greenstone belts which constitute up to 20 vol.% of the upper crust of the WAC (Attoh and Ekwueme, 1997). In the Leo-Man shield, representing the southern part of the WAC (Fig. 1), individual belts of predominantly mafic volcanic rocks extend for ~500 km and are separated from each other by metasedimentary belts up to 200 km wide. In addition to basaltic lava flows, the Birimian greenstone belts typically contain significant andesitic–dacitic pyroclastic rocks, as do the metasedimentary belts which contain significant thicknesses of volcanogenic sediments including fine-grained fragmental volcanic rocks. Chemical sediments composed of manganesestones and chert are interstratified with the Birimian volcanic rocks. This lithologic association, together with the geochemical characteristics of the volcanic rocks, were interpreted as indicating that the Birimian greenstone belts formed in oceanic island arc environments (Sylvester and Attoh, 1992; Evans et al., 1996) similar to those inferred for the Late Archean Superior craton (Sylvester et al., 1987; Card, 1990; Polat and Kerrich, 2001).

In the Dixcove greenstone belt (Fig. 1, belt 1) the overall NNE synclinal structure is cored by fluviatile sediments composed of coarse clastics which overlie the volcanic section. Fig. 2 shows the main volcanic and plutonic rocks of the study area, representing the southern segment of belt 1, located along the coastal section of southwestern Ghana. In this area, the lower part of the volcanic section consists of 2000 m of pillowed basalts and aquagene tuffs exposed east of Dixcove which are inferred to be inter-bedded with manganesestones composed of chert, manganese oxide and carbonate minerals. This succession is similar to that in Nangodi (belt 2, Fig. 1) where the volcanic section consists of 2000 m of tholeiitic basalts followed by 3000 m of andesitic–dacitic pyroclastic rocks (Attoh, 1982). The Dixcove volcanic section was intruded by large granitoid plutons which include the Prince's Town granite and Dixcove granodiorite (Bartholomew, 1991; Loh et al., 1995). These plutons, together with available age data compiled for the southeastern part of the West African craton (e.g., Attoh and Ekwueme, 1997; Evans, 1997) provide a tight constraint on the age of the ultramafic rocks and the greenstone belt volcanics.

## 3. U–Pb ages of Dixcove belt rocks

U–Pb zircon ages have been reported for migmatites and granitoids located on the eastern margin of the

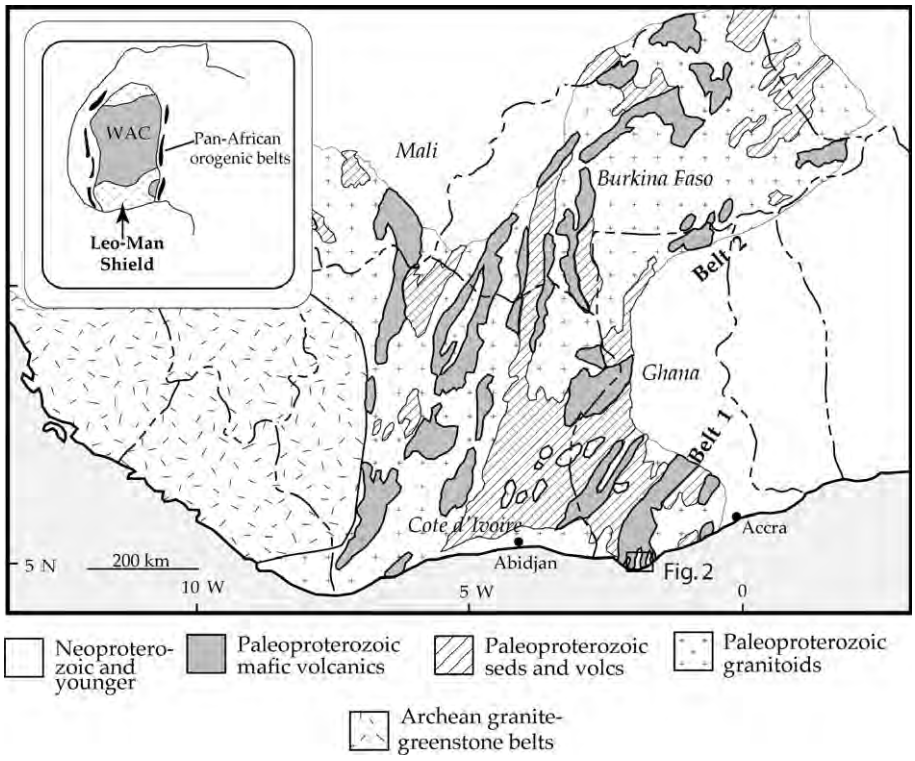


Fig. 1. Paleoprtoterozoic (Birimian) greenstone belts showing location of Dixcove belt study area (outlined by Fig. 2) in the Leo-Man shield of the WAC (inset).

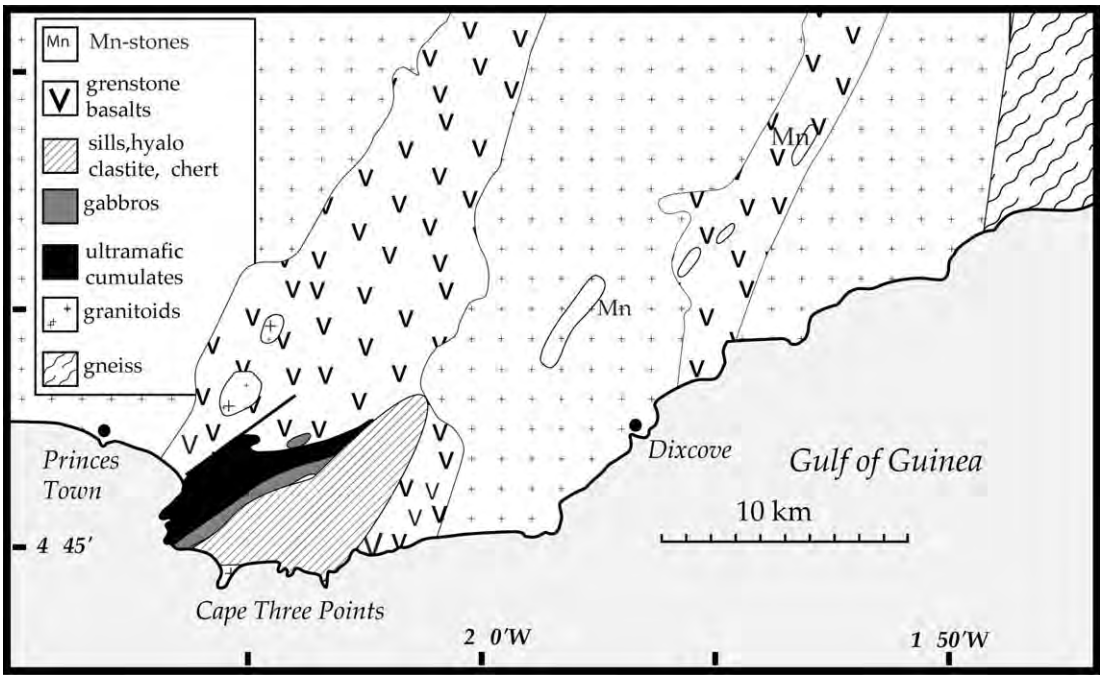


Fig. 2. Geologic map of the Dixcove belt study area (modified after Bartholomew, 1991; Loh et al., 1995).

Dixcove belt by Opare-Addo et al. (1993). They determined an age of 2172 ± 4 Ma which is identical to the one obtained by Hirdes et al. (1992) for the Dixcove granitoid complex (Fig. 2). This age is distinctly younger than 2266 ± 2 Ma age from analysis of a single zircon separated from a felsic pyroclastic unit (Loh et al., 1995). The pyroclastic unit is interpreted to be inter-stratified with the greenstones and intruded by the Dixcove granitoids.

For this study, zircons were separated from the Prince's Town granodiorite (BPD61) which intruded the western flank of the greenstone-ultramafic complex. These were abraded to enhance concordance and analyzed by standard methods of isotope dilution and thermal ionization mass spectrometry (TIMS) in the isotope geochemistry laboratory at Syracuse University. Four multigrain magnetic fractions were analyzed, yielding the data given in Table 1. Fractions m1, m2, and m3 are nearly concordant on a $^{206}Pb/^{238}U$ vs $^{207}Pb/^{235}U$ (concordia) plot and when regressed with the rather discordant least magnetic fraction (nm1) yielded an upper intercept age of 2159 ± 4 Ma with a lower intercept of essentially zero (Fig. 3). This age is younger than that of the Dixcove granitoids on the eastern margin and consistent with the post-tectonic field relations of the Prince's Town granitoid which typically displays

Table 1
Isotopic data for U–Pb analyses of zircon from Prince's Cove granite

| Samples BPD-61[a] | Concentrations[b] | | | Isotopic | Compositions[c] | | Radiogenic ratios[d] | | | Rho[e] | Ages (Ma)[f] | | |
|---|---|---|---|---|---|---|---|---|---|---|---|---|---|
| | Wt (mg) | U (ppm) | Pb (ppm) | $^{206}Pb/^{204}Pb$ | $^{207}Pb/^{206}Pb$ | $^{208}Pb/^{206}Pb$ | $^{206}Pb/^{238}U$ | $^{207}Pb/^{235}U$ | $^{207}Pb/^{206}Pb$ | | $^{206}Pb/^{238}U$ | $^{207}Pb/^{235}U$ | $^{207}Pb/^{206}Pb$ |
| nm(1) | 0.108 | 113.7 | 34.46 | 0.11159 ± 68 | 0.13541 ± 0.00005 | 0.13855 ± 0.00005 | 0.27651 ± 0.00138 | 5.13881 ± 0.02585 | 0.13479 ± 0.00009 | 0.99208 | 1574 ± 8 | 1842 ± 9 | 2161 ± 1 |
| m(1) | 0.124 | 149.5 | 64.06 | 0.18493 ± 77 | 0.13484 ± 0.00003 | 0.13766 ± 0.00003 | 0.39131 ± 0.00185 | 7.25655 ± 0.03461 | 0.13451 ± 0.00007 | 0.99347 | 2129 ± 10 | 2143 ± 10 | 2157 ± 1 |
| m(2) | 0.054 | 187.8 | 78.29 | 0.17096 ± 80 | 0.13512 ± 0.00002 | 0.13533 ± 0.00003 | 0.38166 ± 0.00194 | 7.08717 ± 0.03628 | 0.13468 ± 0.00071 | 0.99451 | 2084 ± 11 | 2122 ± 11 | 2160 ± 1 |
| m(3) | 0.111 | 113.6 | 49.52 | 0.21541 ± 4.4 | 0.14025 ± 0.00004 | 0.14764 ± 0.00005 | 0.39069 ± 0.00189 | 7.25539 ± 0.03541 | 0.13469 ± 0.00008 | 0.99226 | 2126 ± 10 | 2143 ± 10 | 2160 ± 1 |

[a] Magnetic fractions; m = magnetic, nm = non-magnetic, numbers indicate side tilt at full field on magnetic separator.
[b] Total U and Pb, corrected for analytical blank.
[c] Measured ratios, not corrected for blank or mass discrimination.
[d] Ratios corrected for 0.15% per amu mass discrimination, 0.01 ng analytical blank, and non-radiogenic Pb (Stacey and Kramers, 1975 model).
[e] Rho is the correlation coefficient for 207/235–206/238.
[f] Errors are absolute and given at 2 sigma are absolute and given at 2 sigma.

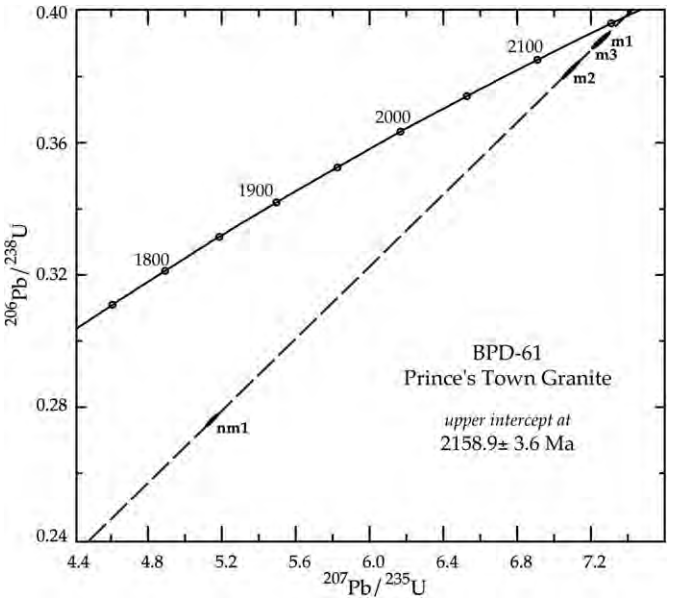


Fig. 3. U–Pb concordia plot of zircon analysis from the Prince's Town granodiorite.

well-preserved, undeformed, magmatic textures. These include porphyritic texture consisting of zoned plagioclase phenocrysts that locally display grain size layering which was interpreted to be the result of gravitational settling (e.g., McCallien, 1955).

## 4. Ultramafic rocks and rodingite field relations

The ultramafic rocks of the Dixcove belt were previously mapped by Bartholomew (1991) and more recently by Loh et al. (1995). They are exposed along a coastal section (Fig. 2) representing the east central synclinal flank of the Dixcove belt. The western contact of the ultramafic complex is faulted and inferred to represent its lower section where it consists of a ~2.0 km thick zone of coarse-grained peridotites, including harzburgite and dunite. Rocks from the ultramafic zone are variably serpentinized where the more intensely altered zones form bays between pointed headlands resulting in a peculiarly jagged coast line. The inferred layering in the ultramafic complex is subparallel to the regional NE strike of the belt and is pronounced in the gabbroic rocks (Fig. 4) which are exposed in the eastern contact zone and interpreted to represent the upper section of the ultramafic complex. The gabbroic rocks include leuco-gabbros, plagiogranite associated with granophyric zones and hornblende-diorite vein rocks along the contact zone.

Rodingite occurs as pods, veins, and blocks in the ultramafic rocks (Fig. 5) and is especially abundant in the vicinity of the highly serpentinized zones indicated by embayment of the coastline (Fig. 2). Rodingite is a distinct rock in outcrop because it is a white-weathering, quartz-poor rock providing a conspicuous contrast with the dark-colored ultramafic host rocks. The largest rodingite outcrops occur as blocks, up to 2 m wide (Fig. 5C and D), but most are a few cm to 1 m across and occur as irregular light-colored patches in the serpentinized peridotite and in the altered gabbroic rocks. The Birimian rodingite occurrence is similar to those reported from ultramafic rocks of other ages and localities, such as in the Archean, where rodingite is associated with serpentinites formed from komatiitic volcanic and sub-volcanic rocks in the Abitibi and Barberton greenstone belts (Schandl et al., 1989; Anhaeusser, 1979). In the Phanerezoic, rodingite occurs in the ultramafic zones of ophiolitic complexes (e.g., Coleman, 1967), has been reported from serpentinized ultramafic intrusions (O'Hanley et al., 1992) and

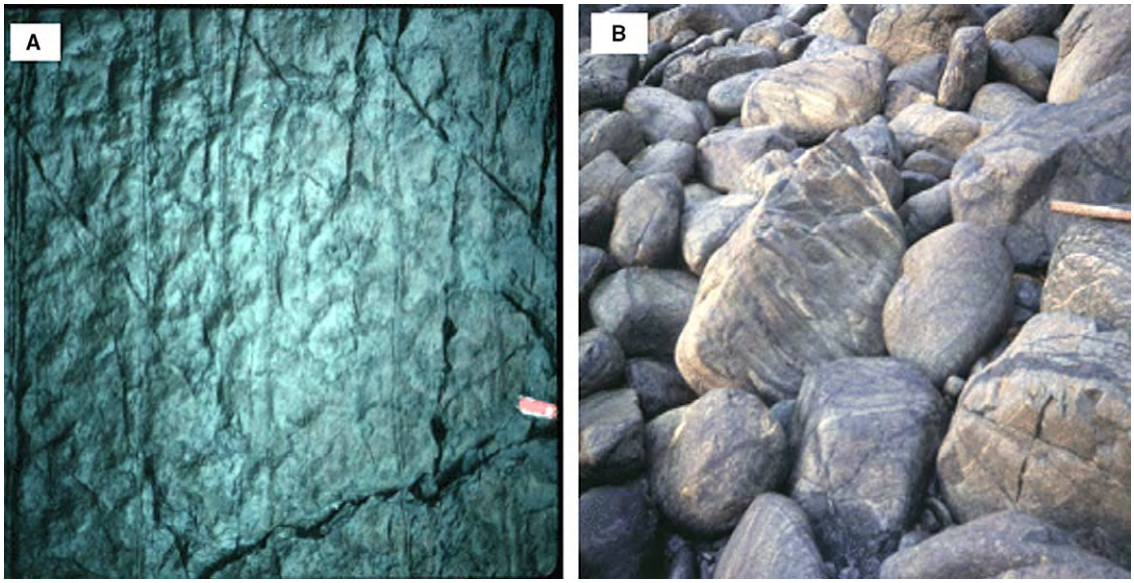


Fig. 4. (A) serpentinized dunite, (B) layering in gabbroic rocks.

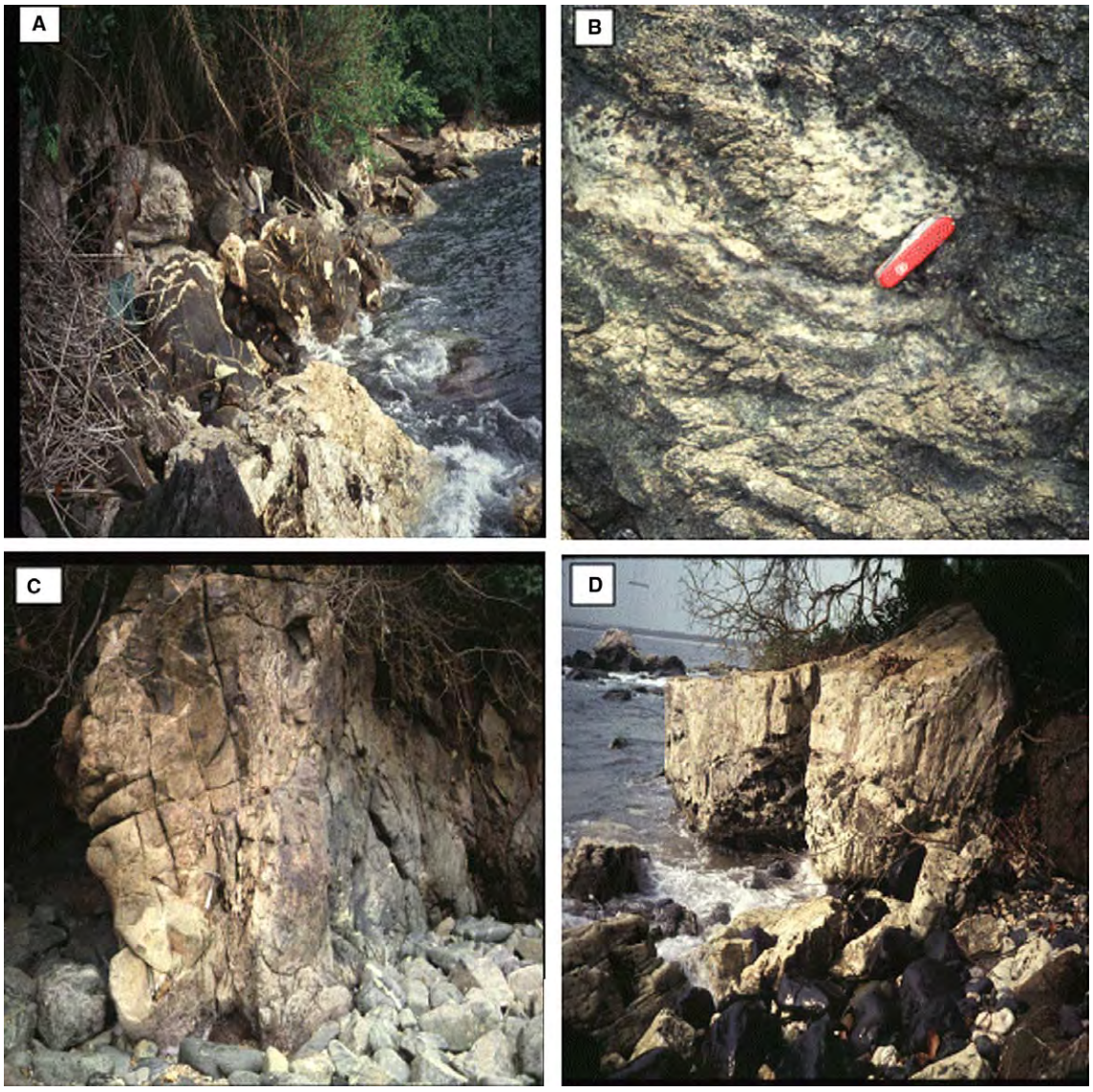


Fig. 5. Rodingite occurrences: (A) veins and pods in serpentinized ultramafic zone (note person, near center, for scale), (B) patches with green spots, (C) and (D) blocks (hammer for scale in C, and in D the block is ~2 thick).

dredged from modern oceanic fracture zones (Honorez and Kirst, 1975). In many of these occurrences, rodingite was interpreted to have formed from a variety of rock types (e.g., gabbros, greywakes) but rarely from the host ultramafic rocks. The field relations for the rodingites described here, however, provide little direct evidence of the protolith from which they formed.

In contact with the gabbroic zone, and inferred to stratigraphically overlie the ultramafic complex, is a unit consisting of basaltic hyaloclastites intercalated with fine-grained sediments including chert and disrupted basaltic-andesitic sills. This unit is interpreted to represent a sheeted-dyke complex and Fig. 6 is a reconstruction of this interpretation which also shows the relations among the principal lithologies associated with the ultramafic complex in the study area. Locations of the samples analyzed are shown in this composite magmatic stratigraphic section proposed to be representative of a cross-section of a Paleoproterozoic oceanic crust.

## 5. Petrography and mineral chemistry

### 5.1. Analytical methods

Standard and polished thin sections were prepared from the ultramafic and rodingite rock samples and studied with the petrographic microscope. Whereas the textures and most of the minerals of the peridotites and gabbros could be identified with the petrographic microscope, the fine-grained texture of the rodingite required the electron microprobe to identify most phases. In addition to identifying minerals, quantitative mineral compositions were obtained on the Cornell electron microprobe (EMP) facility using natural mineral standards. EMP

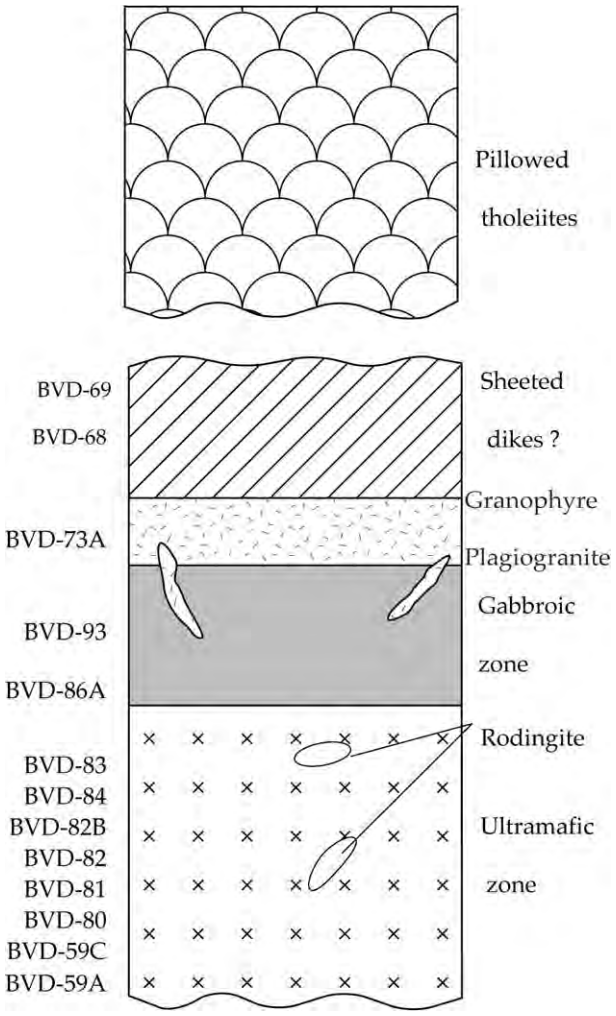


Fig. 6. Reconstructed stratigraphic section of lithologies within the ultramafic–mafic complex showing location of samples discussed in text.

operating conditions were 15 kV with beam currents from 15 to 40 nA.

### 5.2. Peridotites and gabbros

The peridotites of the ultramafic zone display variable degrees of serpentinization but rare primary olivine and orthopyroxene are preserved in some samples (Fig. 7A). In thin section the olivine displays cumulate texture consisting of somewhat rounded, suhedral grains outlined by chromite. Some cumulate grains have reaction rims consisting of orthopyroxene which is typically serpentinized or altered to actinolite. Primary olivine is magnesian (Fo85) with limited compositional range in the preserved grain centers analyzed. Orthopyroxene (Opx) is the primary mineral of the lowermost exposed zone. It occurs in thin section as oikocrysts, poikilitically enclosing cumulate olivine grains. This texture suggests adcumulus formation of Opx which contrasts with the predominance of olivine cumulate in the dunite zone characterized by intense serpentinization (e.g., Fig. 4A). Orthopyroxene displays a narrow compositional range around En86. Fig. 7A shows that despite the intense serpentinization primary magmatic textures can be discerned in thin section. X-ray diffraction analysis showed that antigorite is the principal serpentine mineral of the dunite whereas the alteration products of the Opx-rich rocks include actinolite, chlorite as well as minor antigorite. Chromite and magnetite with high Ni and Co contents are the common opaque minerals and are well preserved in the altered samples.

### 5.3. Rodingites

In hand samples the rodingites are dense, fine-grained rocks displaying color variation due to mineral zones as well as the characteristic pink weathering zones observed in other localities (e.g., Frost, 1975; O'Hanley et al., 1992). In thin section, the green mineral zones are discontinuous with variable amounts of epidote minerals that locally alternate with very fine zoisite or clusters of coarser actinolite (Fig. 7B and C). Outside the localized alternating green mineral zones the bulk of the rodingite is typically very fine-grained; in thin section, these fine-grained areas are nearly opaque (Fig. 7B) but reveal ghost textures suggestive of primary plagioclase laths which have been apparently altered to the calc-silicate minerals. Individual mineral phases identified and analyzed are further described below.

Zoisite occurs as fine-grained crystals that are typically less than 0.1 mm but large grains reach up to 0.4 mm. Table 2 lists zoisite compositions in representative samples and these can be expressed by the formula $Ca_{1.9–2.3}Al_{2.93–2.98}(Si_{3.0–2.96}Al_{.04})O_{12}$. Epidote occurs as part of the fine-grained groundmass, in discontinuous layers and as veins (Fig. 7B) which range in thickness (0.1–0.5 mm). In the thickest veins, individual crystals project from the wall into the vein center with pyramidal terminations suggesting they may have formed from vug filling fluids. Epidote compositions are more variable than zoisite; for example, vein epidote (vEP in Table 2) is more Fe-rich than groundmass epidote and zoisite.

Actinolite occurs as individual or clusters of acicular or stubby grains which are relatively coarse and appear as green specks in which individual grains reach up to 1.5 mm across. Zoning in the coarsest actinolite is suggested by shades of gray in backscattered electron images reflecting slight but measurable Ca or Fe variation. Analyzed actinolites show the variable amounts of Fe and also Al (Table 2). However, the formulae calculated on the basis of 11.5 or 12 oxygens are stoichiometric. The stubby prismatic habit of some actinolite grains (Fig. 7C) suggest they may have formed by replacement of primary pyroxene and this may partly explain their variable composition. The inferred replacement of Opx or other pyroxenes in the peridotites and the rodingite protoliths by actinolite may represent an early stage of Ca metasomatism, especially in the peridotites. Chlorite is a common mineral in the rodingites especially in the ''blackwall' zones and X-ray analysis

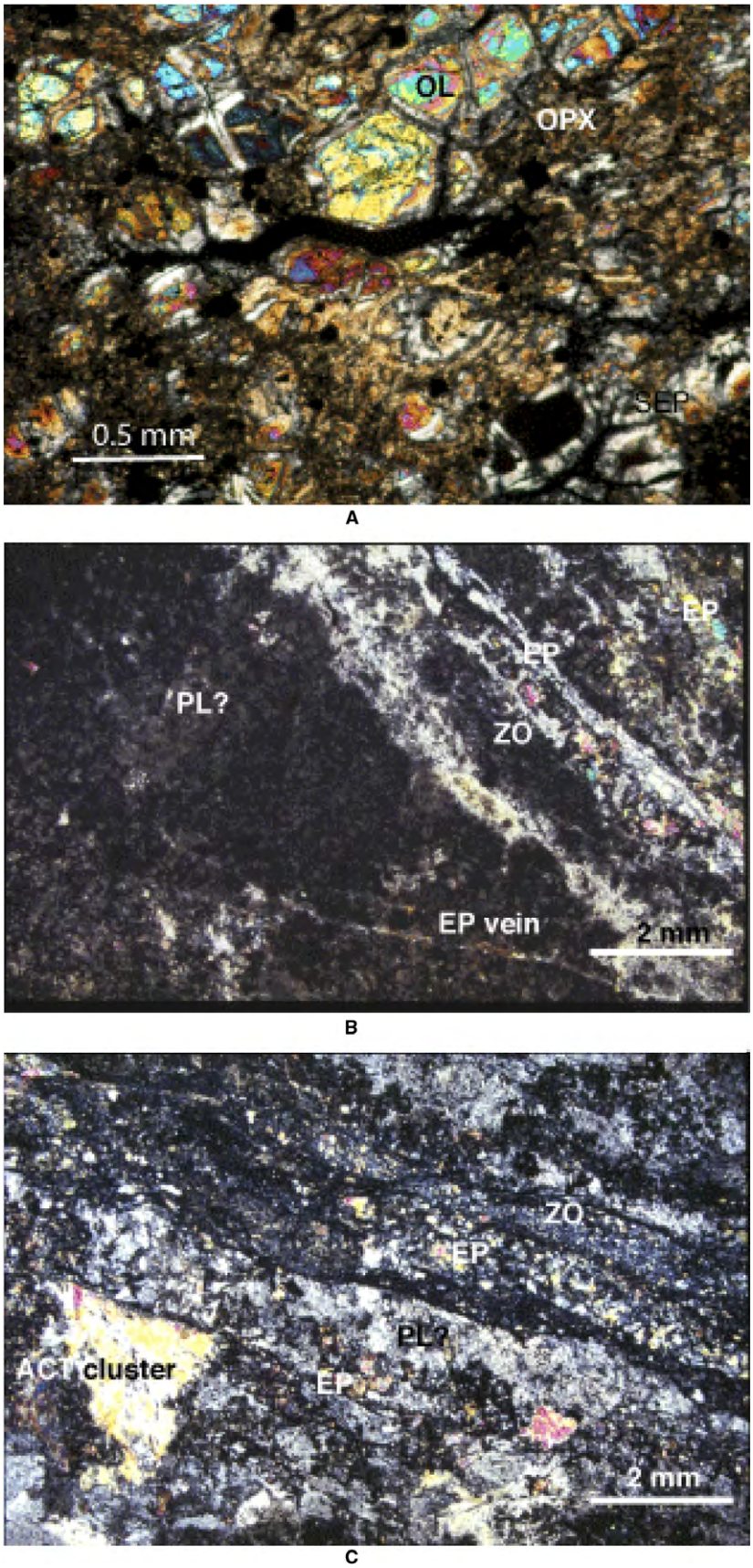


Fig. 7. Photomicrographs: (A) serpentinized harzburgite with relict olivine (Ol) set in highly altered orthopyroxene (Opx). SEP = serpentine. (B) Rodingite consisting of zoisite (ZO) and epidote (EP) layers and nearly-opaque, very fine-grained zone with epidote vein. (C) Alternating zoizite and epidote layering in rodingite with clusters of actinolite (ACT) and 'ghost' plagioclase (PL?).

Table 2
Compositions of representative minerals in rodingites

| | BVD 94D ZO | BVD 94D EP | BVD 94D PRE | BVD 94C ZO | BVD 94C EP | BVD 94C ACT | BVD 87C ZO | BVD 87C EP | BVD 87C vEP | BVD 87C ACT | BVD 87C CHL |
|---|---|---|---|---|---|---|---|---|---|---|---|
| $SiO_2$ | 39.26 | 39.33 | 44.99 | 39.76 | 38.06 | 54.62 | 40.13 | 39.09 | 39.09 | 51.98 | 30.16 |
| $TiO_2$ | 0.03 | 0.0 | 0.02 | 0.12 | 0.15 | 0.18 | 0.06 | 0.00 | 0.04 | 0.06 | 0.01 |
| $Al_2O_3$ | 33.48 | 28.96 | 26.07 | 32.89 | 25.73 | 2.37 | 33.99 | 28.45 | 28.56 | 6.02 | 23.23 |
| $Fe_2O_3$ | 1.84 | 1.22 | 0.04 | 1.76 | 11.86 | | 0.87 | 1.58 | 8.04 | | |
| FeO | | | | | | 10.3 | | | | 9.46 | 14.32 |
| MnO | 0.02 | 0.09 | 0.03 | 0.16 | 0.30 | 0.31 | 0.05 | 0.10 | 0.36 | 0.26 | 0.22 |
| MgO | 0.03 | 3.72 | 0.0 | 0.07 | 0.03 | 17.63 | 0.13 | 2.87 | 0.07 | 17.31 | 26.11 |
| CaO | 24.96 | 24.16 | 27.29 | 23.75 | 23.62 | 13.13 | 24.41 | 24.08 | 23.39 | 12.78 | 0.03 |
| $Na_2O$ | 0.01 | 0.01 | 0.02 | 0.11 | 0.01 | 0.20 | 0.15 | 0.14 | 0.03 | 0.56 | 0.10 |
| Tot. | 99.60 | 97.48 | 98.49 | 98.62 | 99.77 | 98.75 | 99.66 | 96.32 | 99.60 | 99.04 | 94.19 |
| No Ox | 12.50 | 12.5 | 12 | 12.5 | 12.5 | 11.5 | 12.5 | 12.5 | 12.5 | 12 | 14 |
| Si | 2.96 | 3.02 | 3.26 | 3.00 | 2.92 | 3.86 | 3.01 | 3.05 | 2.99 | 3.83 | 2.77 |
| $Al^{IV}$ | | | | | | 0.14 | | | | 0.17 | 1.23 |
| $Al^{VI}$ | 2.98 | 2.63 | 2.22 | 2.93 | 2.35 | 0.06 | 2.98 | 2.61 | 2.57 | 0.35 | 1.29 |
| $Fe^{3+}$ | 0.08 | 0.07 | | 0.10 | 0.69 | | 0.05 | 0.09 | 0.46 | | |
| Ti | 0.0 | 0.0 | | 0.01 | 0.01 | 0.01 | 0.0 | 0.0 | 0.0 | 0.0 | |
| Mg | 0.01 | 0.43 | 0.00 | 0.01 | 0.0 | 1.85 | 0.01 | 0.33 | 0.01 | 1.90 | 3.57 |
| Ca | 2.01 | 2.00 | 2.13 | 1.92 | 1.99 | 0.99 | 1.95 | 2.01 | 1.92 | 1.01 | |
| $Fe^{2+}$ | | | | | | 0.73 | | | | 0.58 | 1.10 |
| Mn | 0.0 | 0.0 | 0.0 | 0.01 | 0.02 | 0.02 | 0.0 | 0.02 | 0.05 | 0.02 | 0.02 |
| Na | 0.0 | 0.0 | 0.0 | 0.01 | 0.0 | 0.02 | 0.0 | 0.0 | 0.0 | 0.08 | |

FeO calculated from $Fe_2O_3$ in actinolite and chlorite.

showed that it is clinochlore which is consistent with the Mg-rich composition listed in Table 2.

Although most previous studies of rodingites list hydrogrossular as a major phase, careful X-ray diffraction analysis, and optical and electron microscopic studies of the Dixcove belt rodingites showed no garnet (grossular or hydrogrossuar). Schandl et al. (1989) showed that hydrogrossular-bearing rodingites apparently formed from epidote-rich ones indicating a metasomatic evolution from epidote-rich to grossular-rich rodingite. The lack of hydrogrossular in the Dixcove belt rodingites may therefore indicate that they have undergone lower extent of rodingitization. This inference is also consistent with the X-ray diffraction results which indicate the preservation of plagioclase as was also noted in the petrography. The composition of plagioclase from the X-ray analysis is calcic-albite ($Na_{.76}Ca_{.19}K_{.05}(Si_{2.8}Al_{1.2})O_8$) and this is consistent with electron microprobe spot analysis of the least altered plagioclase which yielded Ab 75–85.

## 6. Geochemistry

### 6.1. Analytical methods

Major and minor elements were determined by XRF analyses (XRAL labs, Ontario) where the elements analyzed were: Si, Ti, Al, Fe, Mn, Mg, Ca, Na, K, P, Sr and Cr. Trace elements were determined by ICPMS at Cornell University (Evans, 1997) and included REE, Rb, Y, Zr, Nb, Cs, Ba, Hf, Ta, Pb, Th and U. Analytical uncertainties for the trace elements averaged ~8.5% and ranged from less than 1.0% (for Cs) to 12% (for Nb). Major and trace element concentrations were determined in 11 representative ultramafic and gabbroic rock samples (Table 3) and 6 rodingite samples (Table 4).

### 6.2. Major and minor elements in the ultramafic rocks

Rocks of the ultramafic-gabbroic suite are characterized by high Mg# values which range from 80 to 83, but samples analyzed show little systematic variation within the inferred magmatic stratigraphy. The concentrations of Na, Ca and Si are inversely correlated with the Mg content in these rocks, with low Na/Mg, Ca/Mg, but high Si/Mg ratios in the gabbros relative to the ratios in the ultramafic rocks. The ultramafic rocks also have lower $Al_2O_3$ contents, and higher MgO, FeO and Cr contents than the gabbros. The gabbroic and related rocks (Table 3) have very low concentrations of $K_2O$ (<0.08 wt%) and $TiO_2$ (0.1–0.14 wt%) compared to rocks of similar $SiO_2$ contents such as basaltic rocks in this greenstone belt (Evans, 1997). This is exemplified by BVD73A, a rock with $SiO_2 = 67.6$ wt%, Mg# = 40 and yet with $K_2O$ of 0.08 wt%. A plot of the Dixcove belt mafic and ultramafic rocks in an $Al_2O_3$–CaO–MgO diagram (Fig. 8A) shows that the samples analyzed plot in the fields outlined by Coleman (1977) for ophiolitic cumulate rocks. The ultramafic–mafic suite also displays a strong, positive correlation between Cr and MgO concentrations as well as between Y and Zr contents (Table 3) whereas the peridotites cluster around high values of Cr and Mg, and intermediate to low Zr–Y values. These features are consistent with olivine and orthopyroxne fractional crystallization in the formation of the peridotites and in the evolution of the gabbroic rocks with very low Rb

Table 3
Major (wt %) and trace element (ppm) concentrations in representative samples of Dixcove belt ultramafic complex

| | BVD 59A H | BVD 59C H | BVD 80 H | BVD 81 H | BVD 82 D | BVD 82B D | BVD 83 D | BVD 84 H | BVD 93 G | BVD 86A G | BVD 73A PG |
|---|---|---|---|---|---|---|---|---|---|---|---|
| $SiO_2$ | 41.4 | 42.5 | 39.7 | 38.8 | 38.3 | 38.7 | 43.6 | 40.9 | 49.9 | 50.2 | 67.6 |
| $TiO_2$ | 0.21 | 0.30 | 0.09 | 0.15 | 0.1 | 0.19 | 0.11 | 0.12 | 0.14 | 0.1 | 0.58 |
| $Al_2O_3$ | 4.38 | 5.89 | 3.10 | 3.0 | 2.74 | 1.80 | 2.81 | 2.89 | 11.3 | 14.5 | 13.3 |
| $Fe_2O_3$ | 13.3 | 13.5 | 13.7 | 14.4 | 14.2 | 14.9 | 12.3 | 13.2 | 6.68 | 6.11 | 6.07 |
| MnO | 0.18 | 0.19 | 0.19 | 0.17 | 0.19 | 0.28 | 0.19 | 0.21 | 0.13 | 0.13 | 0.07 |
| MgO | 27.5 | 26.9 | 32.4 | 32.4 | 33.7 | 33.4 | 30.2 | 31.6 | 15.3 | 13.2 | 2.07 |
| CaO | 2.97 | 3.96 | 1.88 | 1.26 | 1.91 | 1.85 | 2.53 | 2.19 | 12.4 | 13.2 | 4.68 |
| $Na_2O$ | 0.29 | 0.43 | 0.14 | 0.19 | 0.14 | 0.16 | 0.19 | 0.16 | 0.55 | 0.81 | 3.8 |
| $K_2O$ | 0.03 | 0.02 | 0.0 | 0.0 | 0.0 | 0.03 | 0.0 | 0.0 | 0.04 | 0.0 | 0.08 |
| $P_2O_5$ | 0.02 | 0.03 | 0.0 | 0.02 | 0.0 | 0.02 | 0.04 | 0.0 | 0.0 | 0.0 | 0.21 |
| $CO_2$ | 0.0 | 0.03 | 0.1 | 0.03 | 0.04 | | 0.15 | 0.02 | 0.0 | 0.0 | 0 |
| LOI | 7.65 | 5.58 | 8.5 | 9.40 | 8.35 | 8.15 | 7.7 | 9.0 | 1.75 | 1.35 | 1.25 |
| Tot. | 97.9 | 98.9 | 99.7 | 99.8 | 99.6 | 99.5 | 99.6 | 99.7 | 98.2 | 99.6 | 99.7 |
| Mg# | 80.4 | 80.0 | 82.4 | 81.8 | 82.4 | 81.6 | 83.0 | 82.6 | 82.1 | 81.1 | 40.3 |
| Cr | 3148 | 3079 | 3763 | 3832 | 4106 | 3900 | 3284 | 3490 | 821 | 342 | 0 |
| Cs | 0.55 | 0.51 | 0.68 | 0.92 | 0.09 | 0.03 | 0.38 | 0.30 | 0.05 | 0.03 | 0.07 |
| Rb | 0.92 | 0.67 | 0.67 | 0.58 | 0.19 | 0.1 | 0.23 | 0.44 | 0.24 | 0.28 | 1.52 |
| Ba | 14.1 | 12.5 | 5.17 | 5.92 | 3.17 | 15.6 | 7.17 | 6.89 | 3.14 | 5.05 | 31.9 |
| Nb | 0.37 | 0.75 | 0.06 | 0.19 | 0.13 | 0.20 | 0.18 | 0.24 | 0.15 | 0.13 | 4.57 |
| Ta | 0.03 | 0.05 | 0.01 | 0.02 | 0.01 | 0.02 | 0.01 | 0.01 | 0.01 | 0.83 | 0.41 |
| Sr | 42 | 49 | 29 | 26 | 23 | 20 | 31 | 26 | 71 | 93 | 141 |
| Hf | 0.29 | 0.52 | 0.09 | 0.19 | 0.11 | 0.28 | 0.13 | 0.15 | 0.07 | 0.07 | 3.08 |
| Zr | 10.1 | 18.2 | 1.97 | 5.53 | 3.31 | 8.09 | 2.87 | 4.24 | 3.59 | 1.91 | 89.9 |
| Y | 4.33 | 7.58 | 1.50 | 3.1 | 1.9 | 3.35 | 2.01 | 2.70 | 3.67 | 3.47 | 40.0 |
| Pb | 4.05 | 1.70 | 1.37 | 1.39 | 0.72 | 0.13 | 1.53 | 1.00 | 0.69 | 0.83 | 1.59 |
| La | 1.00 | 1.3 | 0.33 | 0.46 | 0.27 | 0.49 | 0.22 | 0.43 | 0.27 | 0.20 | 12.5 |
| Ce | 2.30 | 3.07 | 0.73 | 1.22 | 0.64 | 1.38 | 0.56 | 0.97 | 0.79 | 0.55 | 27.9 |
| Pr | 0.34 | 0.51 | 0.11 | 0.21 | 0.10 | 0.23 | 0.10 | 0.15 | 0.14 | 0.10 | 4.1 |
| Nd | 1.49 | 2.26 | 0.34 | 0.84 | 0.48 | 1.02 | 0.40 | 0.67 | 0.73 | 0.54 | 18.4 |
| Sm | 0.41 | 0.66 | 0.14 | 0.3 | 0.14 | 0.37 | 0.17 | 0.20 | 0.27 | 0.22 | 4.9 |
| Eu | 0.15 | 0.25 | 0.09 | 0.11 | 0.07 | 0.11 | 0.08 | 0.08 | 0.12 | 0.13 | 1.2 |
| Gd | 0.57 | 0.95 | 0.21 | 0.42 | 0.24 | 0.51 | 0.26 | 0.31 | 0.44 | 0.38 | 5.9 |
| Tb | 0.11 | 0.17 | 0.04 | 0.08 | 0.04 | 0.09 | 0.05 | 0.06 | 0.09 | 0.08 | 1.1 |
| Dy | 0.71 | 1.12 | 0.27 | 0.51 | 0.31 | 0.62 | 0.37 | 0.40 | 0.61 | 0.55 | 7.00 |
| Ho | 0.16 | 0.26 | 0.07 | 0.12 | 0.08 | 0.14 | 0.09 | 0.10 | 0.14 | 0.13 | 1.6 |
| Er | 0.47 | 0.74 | 0.21 | 0.35 | 0.22 | 0.40 | 0.27 | 0.27 | 0.39 | 0.36 | 4.3 |
| Tm | 0.08 | 0.12 | 0.04 | 0.06 | 0.04 | 0.06 | 0.05 | 0.05 | 0.06 | 0.06 | 0.7 |
| Yb | 0.51 | 0.75 | 0.25 | 0.37 | 0.24 | 0.39 | 0.31 | 0.32 | 0.41 | 0.35 | 4.4 |
| Lu | 0.08 | 0.12 | 0.04 | 0.06 | 0.04 | 0.06 | 0.05 | 0.06 | 0.06 | 0.05 | 0.7 |
| Th | 0.11 | 0.12 | nd | nd | 0.02 | nd | nd | 0.05 | 0.03 | 0.02 | 0.9 |
| U | 0.03 | 0.03 | nd | nd | 0.01 | nd | nd | 0.02 | 0.01 | 0.01 | 0.4 |

(H = harzburgite, D = dunite, G = gabbro, PG = plagiogranite).

and Ba contents. High-field strength element (Zr, Nb, Ta) concentrations in the gabbroic rocks are also low but similar to those in the peridotites whereas Sr contents of the gabbroic rocks are distinctly higher indicating plagioclase cumulate in their modes.

### 6.3. Major and minor elements in the rodingites

The rodingites are silica-poor rocks ($SiO_2$ = 43–49 wt%) characterized by high $Al_2O_3$, CaO, and low $K_2O$, MgO and $TiO_2$ concentrations compared to igneous protoliths with similar $SiO_2$ content. Fig. 8B is an AFC diagram of rodingites from the Dixcove belt compared with rodingites reported in the literature (O'Hanley, 1997 and references therein). It shows that rocks identified by previous workers as rodingite are quite variable in composition and that the Birimian Dixcove belt samples are well within this compositional range. The relatively high $Al_2O_3$ contents of the Birimian rodingites are especially similar to those analyzed from Cassiar (British Columbia) by O'Hanley et al. (1992) and plot between the garnetite and prehnitised gabbro analyses for the Lizard Complex of Cornwall, UK (Hall and Ahmed, 1984). Thus the Dixcove belt rodingites may represent intermediate stage of leaching and or Ca-enrichment between the garnetite, thought to represent the product of more extreme leaching, and prehnitised gabbro from Cornwall. This observation may also explain the absence of grossular in the samples studied. Compared to Birimian rodingites, those from the Atlantic fracture zones (Honorez and Kirst, 1975) and Liguria, Italian Alps (Barriga and Fyfe, 1983) are relatively low in Ca and Al but fall within the broad rodingite field (Fig. 8B) outlined by Coleman

Table 4
Major (wt%) and trace element (ppm) concentrations in rodingites

| | BVD 94 | BVD 94B | BVD 94C | BVD 87 | BVD 87B | BVD 87C |
|---|---|---|---|---|---|---|
| $SiO_2$ | 43.2 | 44.4 | 46.3 | 49.2 | 46.8 | 48.7 |
| $TiO_2$ | 0.02 | 0.02 | 0.07 | 0.08 | 0.07 | 0.09 |
| $Al_2O_3$ | 28.9 | 27.0 | 28.3 | 24.1 | 26.6 | 21.8 |
| $Fe_2O_3$ | 1.04 | 1.77 | 1.95 | 3.26 | 2.17 | 4.32 |
| MnO | 0.04 | 0.05 | 0.04 | 0.07 | 0.11 | 0.09 |
| MgO | 0.99 | 2.28 | 1.72 | 2.88 | 2.18 | 4.18 |
| CaO | 21.0 | 18.3 | 16.9 | 13.5 | 14.3 | 13.0 |
| $Na_2O$ | 0.88 | 0.57 | 2.26 | 3.53 | 3.18 | 2.95 |
| $K_2O$ | 0.11 | 0.0 | 0.13 | 0.29 | 0.2 | 0.33 |
| $CO_2$ | 0 | 0.07 | 0.06 | 0 | 0.07 | 0.12 |
| LOI | 2.65 | 3.15 | 2.70 | 1.55 | 2.45 | 2.15 |
| Tot. | 98.8 | 97.5 | 100 | 98.4 | 98.1 | 97.6 |
| Mg# | 65.4 | 71.8 | 63.6 | 63.6 | 66.6 | 65.7 |
| Cs | 0.19 | 0.05 | 001 | 0.02 | 0.01 | 0.01 |
| Ba | 22.5 | 6.29 | 35.6 | 77.3 | 44.6 | 76.6 |
| Ta | 0.01 | 0.00 | 0.01 | 0.02 | 0.04 | 0.05 |
| Sr | 203 | 215 | 202 | 216 | 221 | 194 |
| Hf | 0.04 | 0.03 | 0.08 | 0.07 | 0.07 | 0.10 |
| La | 0.32 | 0.19 | 0.61 | 0.51 | 0.46 | 0.46 |
| Ce | 0.26 | 0.17 | 0.52 | 0.45 | 0.43 | 0.40 |
| Pr | 0.24 | 0.15 | 0.49 | 0.43 | 0.41 | 0.39 |
| Nd | 0.19 | 0.15 | 0.44 | 0.39 | 0.38 | 0.38 |
| Sm | 0.14 | 0.14 | 0.34 | 0.35 | 0.32 | 0.34 |
| Eu | 0.55 | 0.67 | 1.02 | 1.02 | 0.87 | 1.14 |
| Gd | 0.11 | 0.13 | 0.31 | 0.35 | 0.31 | 0.38 |
| Tb | 0.08 | 0.11 | 0.26 | 0.33 | 0.28 | 0.34 |
| Dy | 0.08 | 0.11 | 0.26 | 0.31 | 0.28 | 0.35 |
| Ho | 0.08 | 0.11 | 0.24 | 0.32 | 0.26 | 0.34 |
| Er | 0.06 | 0.10 | 0.22 | 0.29 | 0.25 | 0.33 |
| Tm | 0.06 | 0.09 | 0.22 | 0.30 | 0.23 | 0.32 |
| Yb | 0.07 | 0.11 | 0.23 | 0.28 | 0.24 | 0.35 |
| Lu | 0.06 | 0.11 | 0.23 | 0.29 | 0.22 | 0.35 |

(1967), Schandl et al. (1989). The variable but relatively high $Na_2O$ content of the Birimian rodingites likely reflects the preservation of albitic plagioclase. The Birimian rodingites are distinctly enriched in Sr and Ba compared to the peridotites and gabbros but also compared to rodingites inferred to be derived from gabbroic protoliths (Hall and Ahmed, 1984). Taken together, however, these chemical characteristics are still compatible with plagioclase-rich protoliths.

### 6.4. REE variations

Fig. 9A is a plot of REE variations in the ultramafic–mafic rocks including two samples from the proposed sheeted dyke complex. The ultramafic rocks display flat, chondrite-normalized trends with absolute concentrations ranging from 0.4 to less than 3 times chondrite values. The most REE-enriched samples are harzburgites (59A and 59C), which are from the lowermost exposed zone. suggesting that a significant section of the lower ultramafic zone may be missing, possibly due to faulting. Three samples (BVD80, BVD82 and BVD83) display minor positive Eu anomalies ($Eu/Eu^* = 1.15–1.5$) indicating that plagioclase was a cumulate phase in their formation, but this contrasts with the dunite sample (BVD82B) which shows a negative Eu anomaly ($Eu/Eu^* = 0.7$). The gabbroic samples (BVD86A, BVD93) from the upper section of the ultramafic complex are also highly depleted in REE contents, characterized by LREE depleted patterns ($La/Sm \sim 0.6$) and display a slight positive Eu anomaly ($Eu/Eu^* = 1.35$). Overall, rocks of the gabbroic zone are highly depleted in REE, with the exception of BVD73A which is enriched, in REE with a pattern similar to plagiogranites associated with ophiolites (Samson et al., 2004). The REE variations in two representative samples BVD68 and BVD69 of the proposed sheeted dyke unit (Fig. 6) are also shown for comparison in Fig. 9A; they are clearly depleted compared to BVD73A but enriched with respect to the cumulate gabbros, and are relatively unfractionated, showing only slight LREE enrichment.

REE variations in the rodingites are displayed in Fig. 9B; they are characterized by moderate LREE enrichment, as $(La/Sm)_N$ ranges from 1.35 to 2.35, but like the ultramafics the rodingites also have low REE concentrations that vary from 0.04 to 1.2 times chondrite-values. The most distinctive aspect of the rodingite REE pattern is the large, positive Eu anomaly, with $Eu/Eu^*$ between 2.8 and 5.0. Positive Eu anomalies have been reported for rodingites elsewhere; for example, Hall and Ahmed (1984) also found strong Eu anomalies in rodingite (garnetite and prehnitised gabbros) as well as in the associated fresh gabbros of the Lizard Complex, which is usually interpreted as a Caledonian ophiolite fragment (see references in Hall and Ahmed, 1984). They concluded that the Eu anomaly in the Lizard Complex rodingites was inherited from the gabbro protolith. Although the field relations in the study area provide no direct evidence for the protolith of the Dixcove belt rodingites, the petrographic evidence presented suggests they may have formed from gabbroic rocks as well. As such, the large positive Eu anomaly may be due to plagioclase content; however, we cannot rule out hydrothermal fluids enriched in Eu and Ca formed by alteration of seafloor basalts and serpentinization reactions as a source.

## 7. Discussion

Rodingites are commonly interpreted to be metasomatic rocks produced by Ca-rich fluids derived from serpentinization reactions in peridotites (Coleman, 1967; O'Hanley, 1997). The process is thought to involve preferential Mg-enrichment in the serpentine minerals which results in the enhanced concentration of $Ca^{++}$ in the expelled serpentinization fluids. Examples of such reactions involving the breakdown of orthopyroxene may be expressed as

$$\underset{(\mathrm{Opx})}{\mathrm{Mg(tr\ Ca)_2Si_2O_6}} + \mathrm{H_2O} = \underset{\text{serpentine(antigorite)}}{\mathrm{Mg_3Si_2O_5(OH)_4}} + \underset{(\text{in fluid})}{\mathrm{Ca^{++}}}$$

Rodingitization thus involves the addition of Ca to a protolith that may include a variety of rock types. Combined fluid inclusion and isotopic studies indicate that rodingite formation takes place around 300 °C and $P(H_2O) \sim 1$ kbar

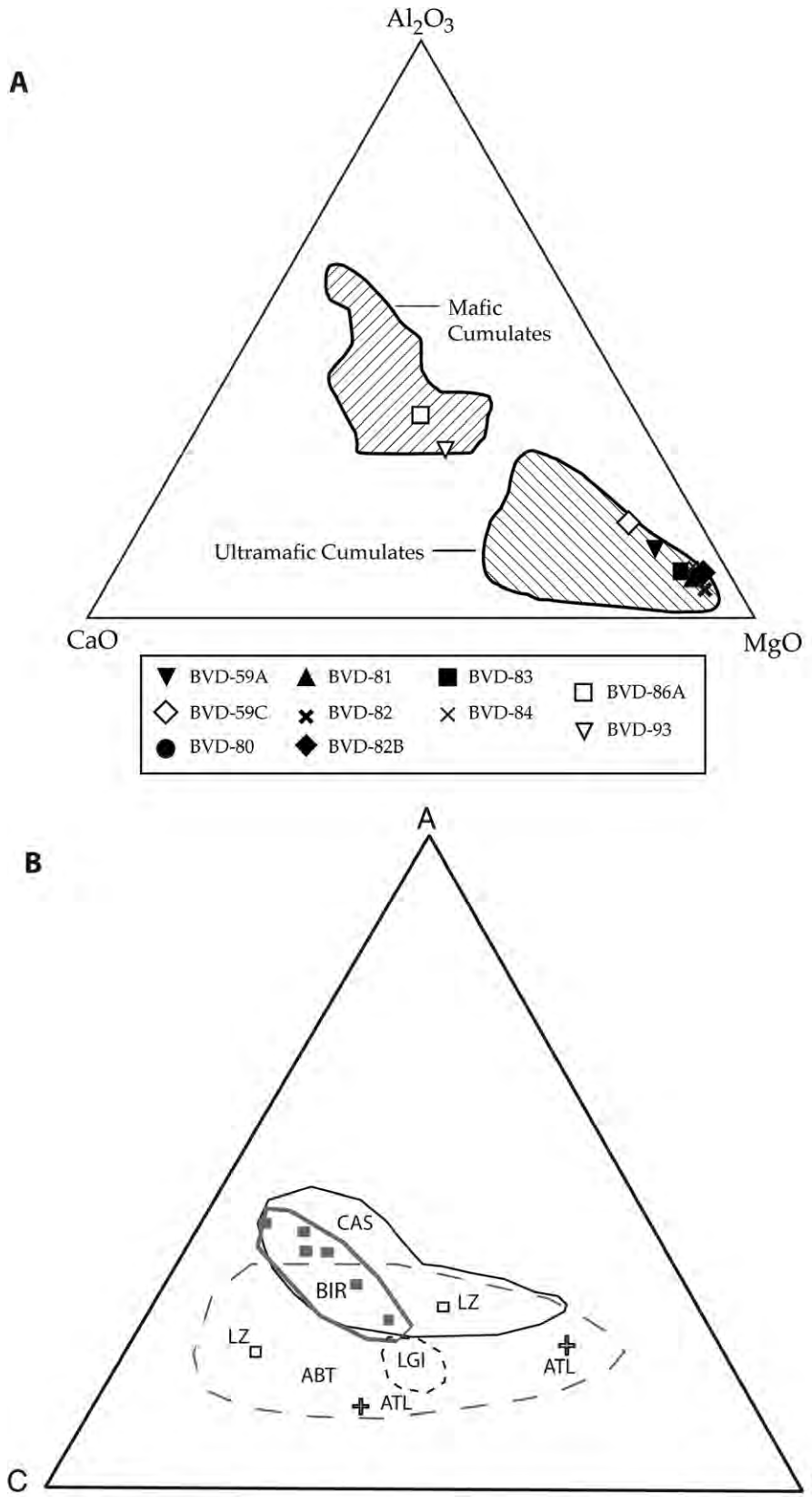


Fig. 8. (A) $Al_2O_3$–CaO–MgO plot of ultramafic and gabbroic rocks compared with ophiolitic rocks (fields after Coleman, 1977). (B) ACF diagram of Birimian rodingites compared with rodingite analyses in references cited in text, BIR (filled squares) = this study; CAS = Cassiar, BC; ABT = Abitibi belt, Ont (broad field outlined by long dashes); LZ = Lizard Complex, UK; LGI = Liguria , Italy; ATL = Atlantic FZ (in ACF :A = $Al_2O_3$–($Na_2O + K_2O$), C = CaO, F = FeO+MgO+MnO).

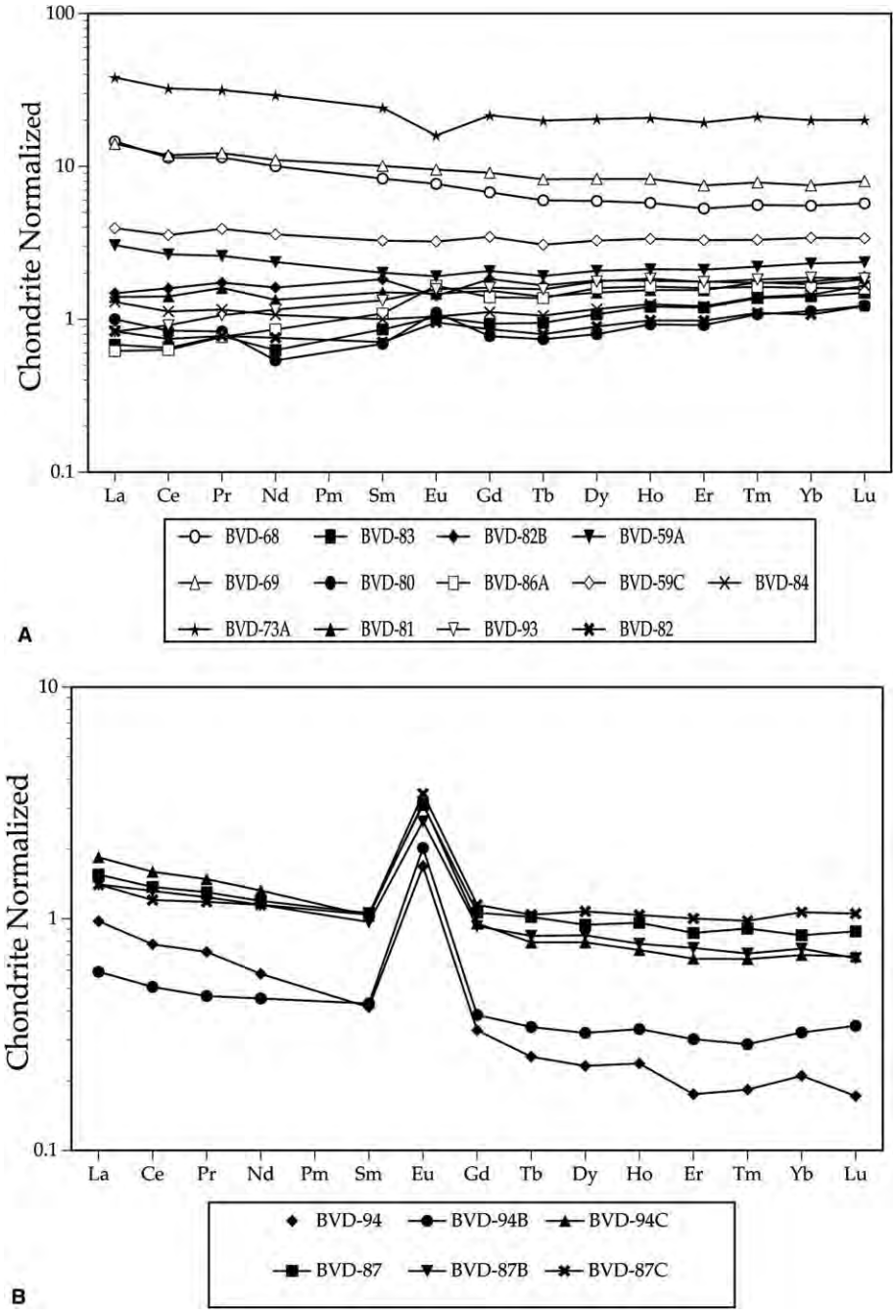


Fig. 9. REE variations in: (A) peridotites and gabbros, including the sheeted dyke complex, (B) rodingites.

(O'Hanley et al., 1992). In the study area, the strong association of the rodingite with serpentinite zones, suggests that they likely formed by metasomatic reactions involving serpentinization fluids. This is supported by the rarity of rodingite in the lower Opx-rich zones where actinolite is the dominant calcic alteration mineral apparently representing an early phase of Ca metasomatism. Serpentinization as the main source of fluids responsible for rodingitization has, however, been challenged by Hall and Ahmed (1984) who proposed that the varied mineral assemblages and REE contents are better explained by non-serpentinizing fluids. They suggested that seawater alteration involving extreme degrees of leaching produced Al-rich rocks such as the garnetites common in some rodingite localities. Here, we propose that the distinct positive Eu anomalies of these rodingites may have been enhanced by interaction of a plagioclase-rich protolith with sea water hydrothermal fluids with its characteristic Eu anomaly (McLennan, 1989).

In addition to providing information on Ca metasomatism during serpentinization, it is significant that nearly all the Phanerozoic rodingite occurrences have been reported from ultramafic rock complexes that are commonly interpreted as ophiolitic bodies (e.g., Hall and

Ahmed, 1984; Coleman, 1977; Schandl and Mittwede, 2001) or modern oceanic crust (Honorez and Kirst, 1975). A similar setting is inferred for the Dixcove belt ultramafic rocks and supported by their ophiolitic affinities. As such, rodingite occurrence in greenstone belts may have important bearing on the tectonic environment where they formed. Although there is some uncertainty about the specific tectonic significance of the Archean rodingite occurrences, the Paleoproterozoic ultramafic-rodingite greenstone belt association described here provides the opportunity to revisit the question about the tectonic setting of the extensive ca 2.1 Ga (Birimian) basaltic magmatism in West Africa.

Current models of Birimian volcanism can be divided into two groups: those favoring plumes (e.g., Abouchami et al., 1990) and those favoring island arc environments (e.g., Sylvester and Attoh, 1992; Evans et al., 1996; Ama Salah et al., 1996). In the plume model, rapid crustal growth was accomplished by a mantle plume event which formed extensive oceanic plateaux. It is envisaged that intra-oceanic subduction was initiated as the plateaux collided with each other or with micro-continental fragments. The island arc setting was inspired by lithostratigraphic constraints and trace element characteristics of Birimian basaltic and fragmental andesitic rocks; it accounts for basalts with MORB affinities to be assembled together with oceanic island arcs during subduction processes. For example, whereas the Birimian basalts in belts 1 and 2 (Fig. 1) have predominant island-arc trace element geochemical signatures (Evans et al., 1996), basalts with transitional-MORB trace element affinities also occur in both belts requiring the West African greenstone belts to be comprised of a collage of accreted oceanic island arc and MORB rocks. Thus all current models of Birimian magmatism are compatible with the operation of Paleoproterozoic subduction-accretion processes in West Africa. Although there is no direct age determination for the Dixcove belt ultramafic–mafic suite, a Paleoproterozoic (Birimian) age is supported by the field relations, as well as the $2159 \pm 4$ Ma age of the granitoid intruded into the western flank of the ultramafic-greenstone belt complex. As such it is proposed that the Dixcove belt ultramafic–rodingite association may represent a fragment of a Paleoproterozoic supra-subduction zone (SSZ) ophiolitic complex. Pearce (2003, and references therein) proposed that SSZ ophiolites are comprised of rock types that formed in back-arc spreading centers and that such rocks tend to have chemical characteristics of volcanic island arcs. This is compatible with the geochemistry of the Birimian basalts where the basaltic pillow lavas have predominant island arc affinities.

## Acknowledgements

This project was supported by grants from Cornell University (1993–1997). KA acknowledges logistical support during fieldwork by the Ghana Geological Survey staff especially Geoffrey Loh. Maura Weathers performed the X-ray diffraction analysis while John Hunt helped with EMP both of which are facilities of the Cornell Center for Materials Research. The paper was significantly improved by the critical comments of two anonymous journal reviewers.

## References

Abouchami, W., Boher, M., Michard, A., Albarede, F., 1990. A major 2.1 Ga event of mantle magmatism in West Africa: an early stage of crustal accretion. Journal of Geophysical Research 95, 17605–17629.

Ama Salah, I., Liégeois, J.-P., Pouclet, A., 1996. Evolution d'un arc insulaire océanique birimien précoce au Liptako nigérien (Sirba): géologie, géochronologie et géochemie. Journal of African Earth Sciences 22, 235–254.

Anhaeusser, C.R., 1979. Rodingite occurrence in some Archean ultramafic complexes in the Barberton Mountain Land. Precambrian Research 6, 49–76.

Attoh, K., 1982. Structure, gravity models, and stratigraphy of an Early Proterozoic volcanic-sedimentary belt in northeastern Ghana. Precambrian Research 18, 275–290.

Attoh, K., Ekwueme, B., 1997. The West African shield. In: De Wit, M.J., Ashwall, L.D. (Eds.), Greenstone Belts. Oxford University Press, pp. 517–528.

Barriga, F., Fyfe, W.S., 1983. Development of rodingite in basaltic rocks in serpentinites, East Liguria, Italy. Contributions to Mineralogy and Petrology 84, 146–151.

Bartholomew, R.W., 1991, The geology of 1/4° field sheets 3 & 5, Axim NE. Ghana. Geol. Survey Archival Report no 18 . Ghana Mineral Commission/GTZ Publication. Accra (in two volumes: vol. 1, 78 pp text, vol. 2, 7 maps and 7 figures).

Card, K.D., 1990. A review of the Superior Province of the Canadian Shield, a product of Archean accretion. Precambrian Research 48, 99–156.

Coleman, R.G., 1967. Low temperature reaction zones and alpine ultramafic rocks of California, Oregon and Washington. USGS Bulletin 1247, 1–49.

Coleman, R.G., 1977. Ophiolites: Ancient Oceanic Lithosphere? Springer-Verlag New York, 229pp.

Condie, K.C., 1997. Plate Tectonics and Crustal Evolution, fourth ed. Butterworth–Heinemann, Oxford, 282pp.

Evans, M.J., 1997. Geochemistry of an early Proterozoic (Birimian) greenstone belt, West Africa. MS thesis, Cornell University, 100pp.

Evans, M.J., Attoh, K., White, W.M., 1996. REE and HFSE concentrations in Early Proterozoic greenstone belts of West Africa: implications for oceanic plateau vs. arc accretion in juvenile crust production. EOS Transactions of American Geophysical Union 77, S291.

Frost, B.R., 1975. Contact metamorphism of serpentinite, chlorite blackwall and rodingite at Paddy-Go-Easy Pass, Central Cascades, Washington. Journal of Petrology 16, 272–313.

Hall, A., Ahmed, Z., 1984. Rare earth content and origin of rodingites. Chemie der Erde 43, 45–56.

Hirdes, W., Davis, D.W., 2002. U–Pb geochronology of Paleoproterozoic rocks in the southern part of the Keougou-Keneba inlier, Senegal, West Africa: evidence for diachronous accretionary development of the Birimain Province. Precambrian Research 118, 83–99.

Hirdes, W., Davis, D.W., Eisenlohr, B.N., 1992. Reassessment of Proterozoic granitoid ages in Ghana on the basis of U–Pb zircon and monazite dating. Precambrian Research 56, 89–96.

Honorez, J., Kirst, P., 1975. Petrology of rodingites from the equatorial mid-Atlantic fracture zones and their geotectonic significance. Contributions to Mineralogy and Petrology 49, 233–275.

Loh, G.W., Hirdes, W., Anani, C., 1995. Geological map of Ghana; Axim and Sekondi Sheets. Geological Survey of Ghana/BGR, Pub., Hanover.

McCallien, W.J., 1955. Gravitational differentiation in small sheets at Prince's Town. Gold Coast – a preliminary statement. Journal of the West African Science Association 1, 62–74.

McLennan, S.M., 1989. Rare earth elements in sedimentary rocks: influence of provenance and sedimentary processes. In: Lipin, B.R., McKay, G.A. (Eds.), Geochemistry and mineralogy of rare earth elements. Reviews in Mineralogy 21, 169–200.

O'Hanley, D.S., 1997. Serpentinites and rodingites as records of metasomatism and fluid history. In: De Wit, M.J., Ashwall, L.D. (Eds.), Greenstone Belts. Oxford University Press, pp. 164–175.

O'Hanley, D.S., Schandl, E.S., Wicks, F.J., 1992. The origin of rodingites from Cassiar, British Columbia and their use to estimate T and P($H_2O$) during serpentinization. Geochimica et Cosmochimica Acta 56, 97–108.

Opare-Addo, E., John, B.E., Mukasa, S.B., Browning, P., 1993. Field and geochronologic (U–Pb) constraints on the age and generation of granitoids and migmatites in southern Ghana. EOS Transactions of American Geophysical Union 74, S301.

Pearce, J.A., 2003. Supra-subduction zone ophiolites: The search for modern analogues. In: Dilek, Y., Newcomb, S. (Eds.), Ophiolite concept and evolution of geological thought. Geological Society of America Special Paper 373, 269–293.

Peters, Tj., Nicolas, A., Coleman, R.G., 1991. Ophiolite Genesis and Evolution of the Oceanic Lithosphere. Kluwer Academic Publishers, Boston, 903pp.

Polat, A., Kerrich, R., 2001. Geodynamic processes, continental growth and mantle evolution recorded in Late Archean greenstone belts of the southern Superior Province, Canada. In: Rollinson, H.R., Whitehouse, M. (Eds.), Archean crustal evolution. Precambrian Research 112, 5–25.

Samson, S.D., Inglis, J.D., D'Lemos, R.S., Admou, H., Blichert-Toft, J., Hefferran, K., 2004. Geochronological, geochemical, and Nd-Hf isotopic constraints on the origin of Neoproterozoic plagiogranites in the Tasriwine ophiolite, Anti-Atlas orogen, Morocco. Precambrian Research 135, 133–147.

Schandl, E.S., Mittwede, S.K., 2001. Evolution of the Acipayam (Denizli, Turkey) rodingites. International Geology Review 43, 611–633.

Schandl, E.S., O'Hanley, D.S., Wicks, F.J., 1989. Rodingites in serperntinised ultramafic rocks of the Abitibi greenstone belt, Ontario. Canadian Mineralogist 27, 579–591.

Stacey, J.S., Kramers, J.D., 1975. Approximation of terrestrial lead isotope evolution by a two-stage model. Earth and Planetary Science Letters 26, 207–211.

Sylvester, P.J., Attoh, K., 1992. Lithostratigraphy and composition of 2.1 Ga greenstone belts of the West African craton and their bearing on crustal evolution and Archean-Proterozoic boundary. Journal of Geology 100, 377–393.

Sylvester, P.J., Attoh, K., Schulz, K.I., 1987. Tectonic setting of Late Archean bimodal volcanism in the Michipicoten (Wawa) greenstone belt, Ontario. Canadian Journal of Earth Sciences 24, 1120–1134.

Taylor, P.N., Moorbath, S., Leube, A., Hirdes, W., 1992. Early Proterozoic crustal evolution in the Birimian of Ghana: constraints from geochronology and isotope geology. Precambrian Research 56, 97–111.